The 2013 World Congress on
Advances in Structural Engineering and Mechanics (ASEM13)
Jeju, Korea, September 8-12, 2013

Influence of Failed Blade Pitch Control System to FOWT by Aero-Elastic-Control-Floater-Mooring Coupled Dynamic Analysis

*Yoon Hyeok Bae[1)] and Moo-Hyun Kim[2)]

[1), 2)] *Department of Civil Engineering, Texas A&M University, College Station, TX, USA*
[1)] *yoonhyeok.bae@tamu.edu*

ABSTRACT

More FOWTs (floating offshore wind turbines) will be installed as relevant regulations and technological hurdles are removed in the coming years. In the present study, a numerical prediction tool has been developed for the fully coupled dynamic analysis of FOWTs in time domain including aero-loading, tower elasticity, blade-rotor dynamics and control, mooring dynamics, and platform motions so that the influence of rotor-control dynamics on the hull-mooring performance and vice versa can be assessed. The developed coupled analysis program is applied to Hywind spar design with 5MW turbine. In case of spar-type floaters, the control strategy significantly influences the hull and mooring dynamics. If one of the control systems fails, the entire dynamic responses of FOWT can be totally different. Therefore, it is important to maintain various control systems of FOWTs in a good operational condition. In this regards, the effects of failed blade pitch control system on FOWT including structural and dynamic response of blades and floater are systematically investigated. Through this study, it is seen that the failure of one of the blade pitch control system can induce significant dynamic loadings on the other blades and the entire FOWT system. The developed technology and numerical tool are readily applicable to any types of floating wind farms in any combinations of irregular waves, dynamic winds, and steady currents.

1. INTRODUCTION

Wind is the fastest-growing clean and renewable energy source. Until recently, most of the wind-farm development has been limited to the land space or shallow-water areas. However, there exist negative features of on-land wind farms that include lack of available space, noise restriction, shade, visual pollution, limited accessibility in mountainous areas, community opposition and regulatory problems.

[1)] Postdoctoral Research Associate
[2)] Professor

In this regard, several countries started to plan floating offshore wind farms. Although they are considered to be more difficult to design, wind farms in deeper waters are in general less sensitive to space availability, noise restriction, visual pollution and regulatory problems. They are also exposed to much stronger and steadier wind field to be more effective. Furthermore, in designing those floating wind farms, the existing technology and experience of offshore oil & gas industry is directly applicable. If the relevant technology and infrastructure are fully developed, offshore floating wind turbines are expected to produce huge amount of clean electricity at a competitive price compared to other energy sources (Henderson et al., 2002; Henderson et al., 2004; Musial et al., 2004; Tong, 1998).

For floating wind turbines, their natural frequencies of 6-DOFs motions are typically much lower than those rotor-induced or tower-flexibility-induced excitations, so the possibility of such dynamic resonance is small (Jonkman and Sclavounos, 2006; Withee, 2004). One exception is the TLP-type OWT (Bae et al., 2010; Jagdale and Ma, 2010) which is much stiffer in the vertical-plane modes compared to other floating wind turbines, and thus the effects of such high-frequency excitations from the tower and blades need to be checked. The second-order sum-frequency wave also induces significant excitation of TLP-type hull when the turbine is in parked condition (Bae and Kim, 2013a). For spar or semi-submersible floaters (Roddier et al., 2009), the low-frequency excitations related to blade pitch-angle control may cause large-amplitude slowly-varying resonant floater motions (Nielsen et al., 2006). Therefore, the accurate estimation of the coupling effects between the floater dynamics and control-induced actuation forces is very important in the optimal design of such floating OWTs.

In this regard, a rotor (aero-elastic-control)-floater-mooring coupled dynamic analysis computer program is developed by combining several modules. For the dynamic analysis and control of wind turbine system, the primary design code of wind turbines FAST developed by National Renewable Energy Laboratory (NREL) is employed (Jonkman, 2003, 2007, 2008; Jonkman and Buhl Jr, 2004). The FAST is implemented into the floater-mooring coupled dynamic analysis program, CHARM3D, which has been developed by authors' group during the past decade (Kim et al., 2001; Tahar and Kim, 2003; Yang and Kim, 2010). They are combined and modified so that the entire system can be solved in time domain by a global combined matrix including all the relevant coupling forces and degrees of freedom. As a result, the dynamic time histories of the FOWT system including full couplings among tower, floater and mooring can be obtained simultaneously by a single run. In this paper, the developed computer program is applied to the analysis of a 5MW spar-type FOWT designed for 320m water depth to study the effects of failed blade-control strategies on the global responses and local structural loadings. The effects of the rotor imbalance induced by the failed blade pitch control are presented in time domain and discussed. Similar research about the dynamic response of TLP-type FOWT with partially broken blade was conducted before (Bae and Kim, 2013b) and it showed that the unbalanced-loadings from the blades may induce additional excitations and responses in the tower and blade dynamics.

2. NUMERICAL ANALYSIS OF 5MW FLOATING WIND TURBINE IN TIME DOMAIN

The time-domain simulation tool for rotor-floater-control-mooring fully-coupled dynamic analysis is developed in this study and it is applied to the 5MW Hywind spar-type FOWT system. In order to couple the wind-turbine elastic motion and the tether/floater dynamics, two different analysis modules, CHARM3D and FAST, are combined to be able to solve their coupling effects simultaneously in a combined matrix of the system. The hydrodynamic coefficients including added mass, radiation damping, wave forces and mean drift forces of floaters are obtained by the 3D diffraction/radiation preprocessor WAMIT in frequency domain (Lee and Newman, 1991) and the information is transferred to the time-domain analysis tool, CHARM3D. The mooring dynamics coupled with hull motions are solved at each time step by a generalized-coordinate-based FEM program using high-order element, the details of which are given in Kim et al. (2001).

The equation of motion of floating body in time domain can be expressed as follows:

$$[M + M^a(\infty)]\ddot{\xi} + K\xi = F_I(t) + F_c(t,\dot{\xi}) + F_n(t,\dot{\xi}) + F_m(t) \tag{1}$$

where $M^a(\infty)$ denotes added mass at infinite frequency, M the system mass matrix, K the system hydrostatic stiffness matrix, $F_I(t)$ the first and second order wave exciting force, $F_n(t,\dot{\xi})$ the nonlinear drag force from Morison's equation at the instantaneous wet position, $F_m(t)$ the mooring force, and $F_c(t,\dot{\xi})$ the radiation damping force as follows:

$$F_c(t,\dot{\xi}) = -\int_{-\infty}^{t} R(t-\tau)\dot{\xi}(\tau)d\tau \tag{2}$$

ξ, $\dot{\xi}$, and $\ddot{\xi}$ represent the 6-DOFs displacements, velocities, and accelerations of the floating body. $R(t)$ is the retardation function.

The complete nonlinear aero elastic equations of motion for the wind turbine model is

$$M(\underline{q},\underline{u},t)\ddot{q} + f(\underline{q},\dot{\underline{q}},\underline{u},\underline{u}_d,t) = \underline{0} \tag{3}$$

where M is the mass matrix, f is the forcing function, $\underline{u}$ and $\underline{u}_d$ are the set of wind turbine control inputs and wind inputs, respectively. $\underline{q}$, $\dot{\underline{q}}$, and $\ddot{\underline{q}}$ are the vectors of wind turbine motions, velocities, and accelerations, and t is time.

The wind turbine dynamics including 6-DOFs platform dynamics are computed by FAST, which is developed by NREL. CHARM3D calculates all of the external forces acting on the platform, and feeds the external forces to FAST at each time step. The transferred external forces include first-order and second order wave forces, radiation damping force, nonlinear viscous drag force from Morison members, and mooring-induced restoring force. The mooring restoring force can be estimated by the top tension of each mooring line and its directional cosine. Then FAST fills out the forcing function in Eq. (3) using those transferred forces, and solves displacements, velocities, and accelerations of all degrees of freedom including elastic responses. Those obtained platform kinematic data are then fed into CHARM3D side in order to update external forces. The procedure is repeated for the next time step. For the present simulation, the time step of CHARM3D-side is 0.05s and the internal time step for FAST-side is 0.0125s, which means that at every time interval of CHARM3D, the FAST internally calculates 4 steps, and return the resultant data to CHARM3D. The basic concept of rotor-floater coupling is schematically shown in Figure 1.

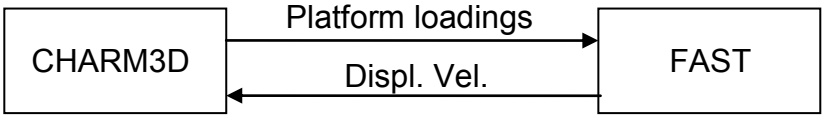

Figure 1 Basic concept of FAST-CHARM3D coupling

The control system of the 5MW wind turbine consists of variable-speed and variable-blade-pitch-to-feather controller. The two control strategies work together to produce quality power and keep the entire system in good condition. Typical control strategies of land-based turbine can directly be applicable to TLP-type offshore wind turbines without any significant modification due to their limited rotational motions (roll, pitch and yaw). However in case of spar-type offshore wind turbines, it is necessary to change the control strategy to ensure smooth operation and higher-quality power generation. In this study, modified control strategy which is optimized for a spar-type FOWT will be used. For the accurate estimation of the global performance of the FOWT system with the respective control strategies, a reliable rotor-floater-mooring coupled dynamic analysis tool is essential.

The adopted model of 5MW turbine is the ‘National Renewable Energy Laboratory (NREL) offshore 5MW baseline wind turbine’ which has been adopted as the reference model for the integrated European UpWind research program. Hywind floating platform in this paper is the ‘OC3-Hywind’ spar-buoy-type platform which is slightly different from the turbine used by Statoil-Norway. The detailed specifications of the 5MW turbine and Hywind spar are tabulated in Tables 1~2.

Table 1 Specifications of 5MW Turbine

Item	Unit	Value
Tower height	m	90.0
Rotor diameter	m	126.0
Tower diameter (top)	m	3.87
Tower diameter (bottom)	m	6.5
Elevation to Tower Base above SWL	m	10.0
Elevation to Tower Top above SWL	m	87.6
Overall Tower mass	kg	249,718
Total wind turbine weight (except for platform)	kg	599,718
CM Location of Tower above SWL Along Tower Centerline	m	43.4
Tower Structural Damping Ratio (All modes)	%	1.0

Table 2 Specifications of Hywind spar platform

Item	Unit	Value
Depth to Platform Base below SWL (Total Draft)	m	120.0
Elevation to Platform Top Above SWL	m	10.0
Depth to Top of Taper Below SWL	m	4.0
Depth to Bottom of Taper Below SWL	m	12.0
Platform Diameter Above Taper	m	6.5
Platform Diameter Below Taper	m	9.4
Platform Mass, including Ballast	kg	7,466,330
CM Location Below SWL Along Platform Centerline	m	89.9155
Platform Roll Inertia about CM	$kg \cdot m^2$	4,229,230,000
Paltform Pitch Inertia about CM	$kg \cdot m^2$	4,229,230,000
Platform Yaw Inertia about Platform Centerline	$kg \cdot m^2$	164,230,000

The Hywind spar is moored by a system of three catenary lines. To increase the yaw stiffness of the platform, the lines are attached to the hull via delta connection. This delta-connection effect is included in the time-domain simulation by adding yaw spring stiffness. The specifications of mooring system are tabulated in Table 3.

Table 3 Specifications of Hywind spar mooring system

Item	Unit	Value
Number of Mooring Lines	ea	3
Angle Between Adjacent Lines	deg	120
Depth to Anchors Below SWL (Water Depth)	m	320
Depth to Fairleads Below SWL	m	70.0
Radius to Anchors from Platform Centerline	m	853.87

Table 3 Continued

Item	Unit	Value
Radius to Fairleads from Platform Centerline	m	5.2
Unstretched Mooring Line Length	m	902.2
Mooring Line Diameter	m	0.09
Equivalent Mooring Line Mass Density	kg/m	77.7066
Equivalent Mooring Line Weight in Water	N/m	698.094
Equivalent Mooring Line Extensional Stiffness	N	384,243,000
Additional Yaw Spring Stiffness	Nm/rad	98,340,000

Each mooring line is modeled by 20 high-order finite elements, and its unstretched length is 902.2m. Illustrations of mooring-line arrangement are shown in Figure 2.

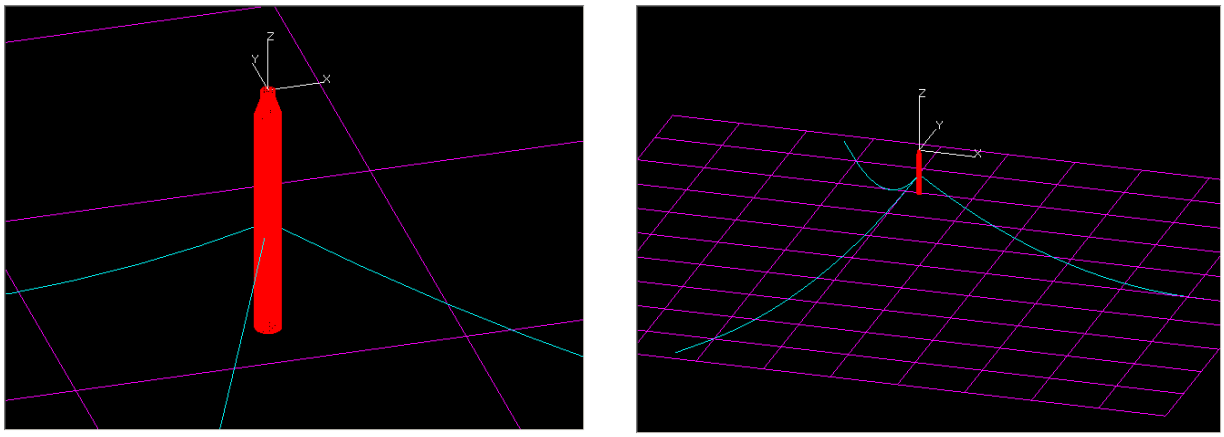

Figure 2 Mooring-line arrangement

The natural frequencies of the Hywind spar platform are tabulated in Table 4.

Table 4 Natural frequencies of platform motions

Mode	Surge	Sway	Heave	Roll	Pitch	Yaw
Frequency (rad/s)	0.05	0.05	0.20	0.22	0.22	0.71

3. FAILURE OF BLADE PITCH CONTROL SYSTEM

For the NREL 5MW turbine, two control systems are designed to work. A generator-torque controller and a blade-pitch controller are working in the below-rated and above-rated wind-speed range respectively. The generator-torque controller is designed to maximize power capture and blade-pitch controller is designed to regulate generator

speed by gain-scheduled proportional-integral (PI) control. In this study, one of the blade pitch actuator is assumed to be locked and does not work while the others work properly as depicted in Figure 3.

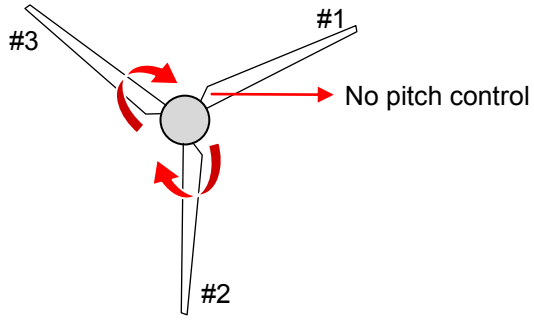

Figure 3 Failed blade pitch control

In time-domain simulation, the total simulation time is set to 1,000 seconds, and the mal-function of the blade pitch control occurs at 100 seconds. The failed blade pitch angle is locked at 100 seconds and fixed for the remaining time. The time histories of blade pitch angle are shown in Figure 4.

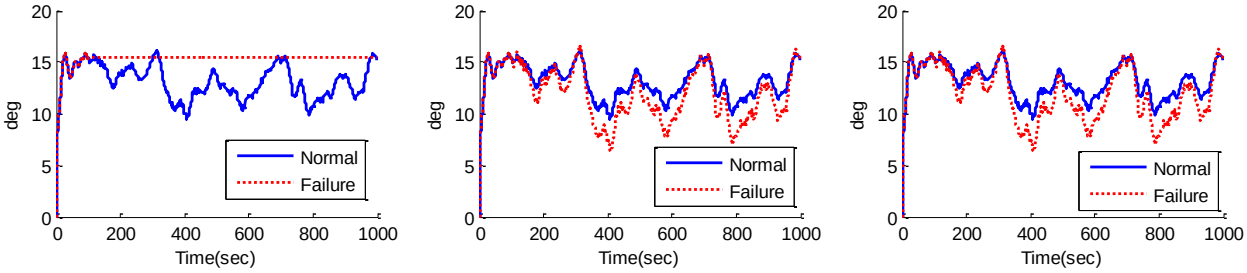

(a) Blade #1 (b) Blade #2 (c) Blade #3

Figure 4 Blade pitch angle with failure after 100 seconds

In Figure 4(a), the blade pitch angle in dotted line is fixed at 15.38 degrees which is the final pitch angle at 100 seconds. Since the pitch angle is fixed at relatively higher angle, the thrust force from the wind decreased accordingly. To maintain the rotor speed and to compensate the loss of thrust force, the other two blades start to lower the pitch angles as can be seen in Figures 4(b)~4(c). For example, the minimum pitch angle of 9.49 degrees in normal condition goes down to 6.39 degrees. As a result, the total thrust force of the rotor remains at a normal level and the decrease of a generated electricity can be minimized.

The changes in the blade pitch angles also affect the blade root shear forces. In the case of blade #1, the overall shear force after failure decreased due to the loss of the

aerodynamic loading, while the other blades show increased mean shear forces as can be seen in Figure 5. The statistics in Table 5 indicate that the mean shear force of blade 1# decreased by 33.3%. On the contrary, the mean shear force of blades #2 and #3 increased 12.3% and 22.5% respectively. The standard deviation of the shear force also increased by 14.0~31.4%, which means the blade roots in failure condition can be subjected to the fatigue damage.

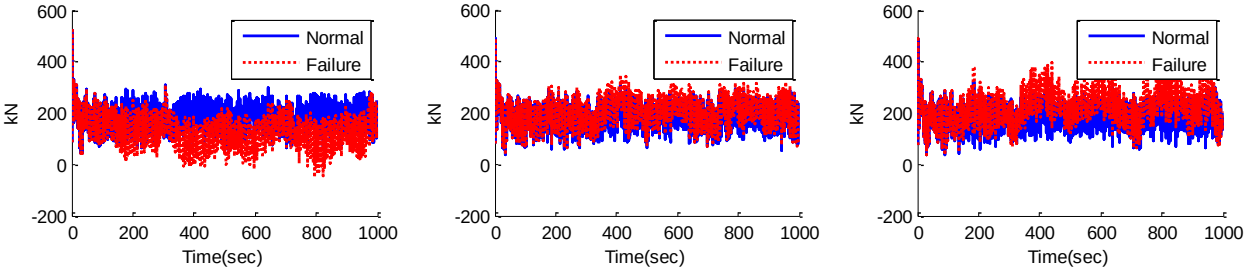

(a) Blade #1 (b) Blade #2 (c) Blade #3

Figure 5 Blade flapwise shear force with failure after 100 seconds

Table 5 Statistics of blade flapwise shear force with failure after 100 seconds

		Max.	Min	Mean	SD
Blade #1 (kN)	Normal	3.082E+02	5.948E+01	1.828E+02	4.250E+01
	Failure	3.104E+02	-5.092E+01	1.219E+02	5.160E+01
Blade #2 (kN)	Normal	3.083E+02	5.253E+01	1.826E+02	4.243E+01
	Failure	3.468E+02	6.472E+01	2.051E+02	4.837E+01
Blade #3 (kN)	Normal	3.185E+02	4.328E+01	1.824E+02	4.315E+01
	Failure	3.946E+02	4.717E+01	2.236E+02	5.668E+01

In the case of maximum and mean shear force between blades #2 and #3, the latter has greater responses. This results are strongly related to the order of blade arrangement and the platform yaw motion induced by asymmetric loadings on the blades. In detail, the blade root shear force is determined by both blade inertial loading and aerodynamic loading. The blade inertial loadings may differ from each blade depending on the instantaneous blade position and the platform yaw acceleration. In this study, the platform yaw period is strongly correlated with the 1P frequency excited by mal-functioned blade #1. 1P represents the once-per-revolution frequency of the rotor (1.27 rad/s) and it can be obtained from the rated rpm (12.1 rpm here). Since rotor frequency and platform yaw frequency are coincide, each blade root shear force shows their repeated pattern and one of the blade shear force can be statistically higher than the others one. This phenomenon is confirmed by yawing turbine model and steady wind test. In figure 6, the azimuth angles of the blades where their root shear force is maximum in steady state condition are depicted. In steady state condition, each blade

always has its maximum shear force near the designated point and each maximum shear force is determined by that instantaneous position, platform yaw acceleration and aerodynamic loading at that time. If the platform yaw motion is restricted or the turbine is land-based, this phenomenon cannot be observed and the maximum or mean level of the blades #2 and #3 will be similar.

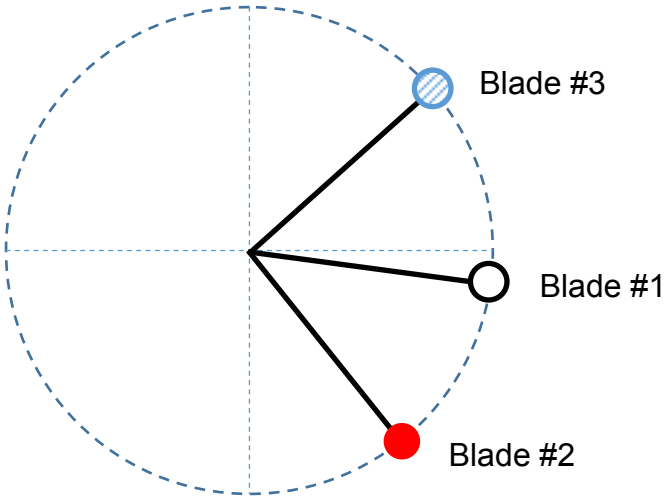

Figure 6 Azimuth point of maximum blade root shear force

Furthermore, the aerodynamic loading on the blades with yawing platform and wind shear along the vertical direction also contribute this trend of the blade root shear forces. In summary, the differences of maximum and mean shear force between blades #2 and #3 are made by the combination of 1P rotation of rotor, 1P yaw motion and inertial loading and aerodynamic loading on each blade.

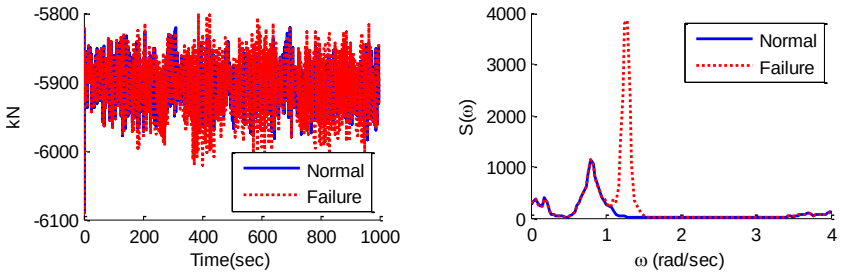

(a) Time history (b) Spectra

Figure 7 Tower base axial force

Due to the imbalance of the blade aero dynamic loadings, the hub may induce the dynamic loadings at the tower base. The tower base vertical loading and torsional

loading in Figures 7~8 show significant changes after failure of blade pitch angle control. Specifically, it has clear resonance peak near 1.27 rad/s, which is associated with the 1P frequency. In case of normal condition, the blades are well balanced and the corresponding effect of 1P excitation is very small or hardly noticeable.

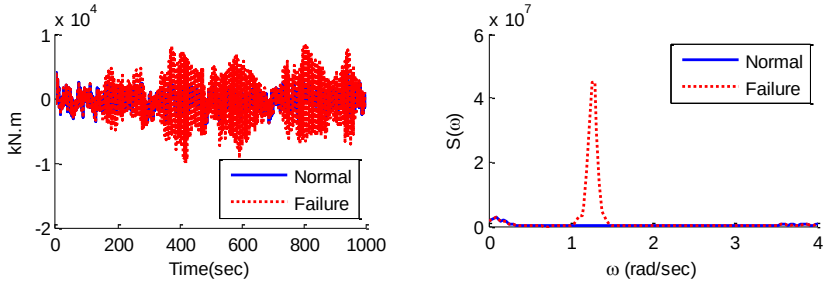

(a) Time history (b) Spectra

Figure 8 Tower base torsional moment

The statistics in Table 6 shows the dramatic changes of torsional moment of tower base between normal and failure case. The maximum torsional moment after failure increased by 96.9% and the maximum of the opposite direction of torsional moment increased up to 138.4%. So, the structural failure of the tower base may occur if the safety factor is not enough to cover these load variations.

Table 6 Statistics of tower base loads

		Max.	Min	Mean	SD
Axial (kN)	Normal	-5.822E+03	-5.985E+03	-5.907E+03	2.439E+01
	Failure	-5.801E+03	-6.021E+03	-5.908E+03	3.413E+01
Torsional (kN·m)	Normal	4.260E+03	-4.240E+03	-3.340E+02	1.087E+03
	Failure	8.389E+03	-1.011E+04	-3.171E+02	2.871E+03

Though the drag force of blade #1 decreased, the overall rotor thrust force shows similar level with the normal case because the deficit of aerodynamic loading from blade #1 is compensated by the other blades. In Figure 9, it is seen that the rotor thrust force after failure does not make big difference except for the very small additional excitation near the 1P frequency.

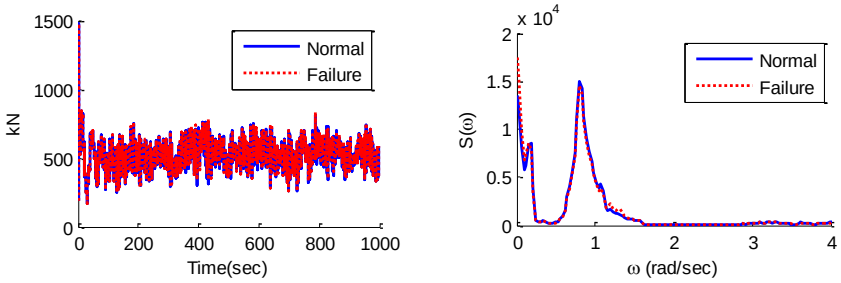

(a) Time history (b) Spectra

Figure 9 Rotor thrust force

The blade pitch failure also affects the dynamic response of floating platform. Figure 10 shows the platform yaw motion and its spectrum. Compared to the normal case, the peak near the 1P frequency is very clear and the variation of the yaw motion is much severe than that of the normal case. Maximum platform yaw angle increased from 1.05 degrees to 2.26 degrees and the standard deviation after failure is higher than that of normal case by 58.9%.

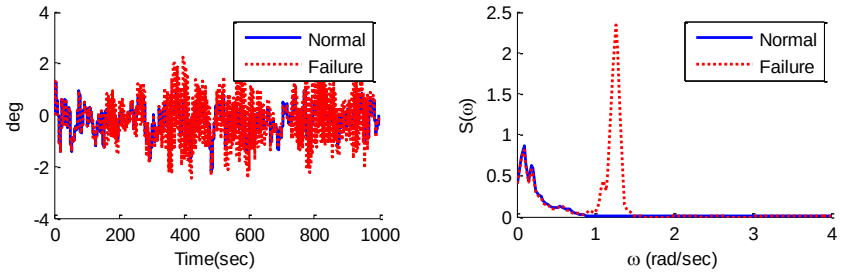

(a) Time history (b) Spectra

Figure 10 Platform yaw motion

So far, the simulation was carried out when the blade pitch angle is locked after 100 seconds. In that simulation, the final pitch angle was 15.38 degrees which reduces the aerodynamic loading on that blade considerably compared to the other blades. The simulation also can be done with different locking time and associated final pitch angle. For example, if the blade pitch actuator is locked at 400 seconds, then the final blade pitch angle is going to be 9.98 degrees which is much lower than the previous case. In this case, the aerodynamic loading on the blade #1 increases and corresponding blade pitch angles of blades #2 and #3 will increase as can be seen in Figure 11.

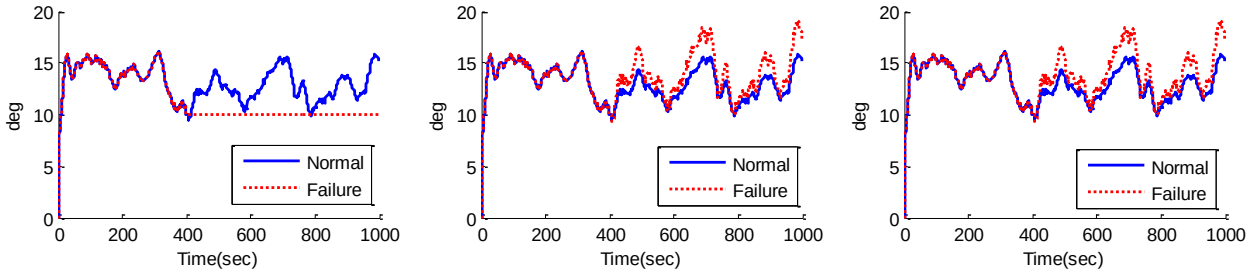

(a) Blade #1 (b) Blade #2 (c) Blade #3

Figure 11 Blade pitch angle with failure after 400 seconds

The resultant blade flapwise shear forces are depicted in Figure 12. The increased aero loading of blade #1 results in the higher shear force, while the shear forces from the other blades show lower mean values compared to the normal case. For instance, the mean shear force of blade #1 increased by 24.9%, while the mean shear forces of the other blades decreased by 8~16.3% as can be seen in Table 7. In this example, the mean and minimum shear forces between blades #2 and #3 after 400 seconds also show noticeable difference and it can be explained in a similar way as pointed out before. Depending on the phase difference between platform yaw motion and the rotor rotation, the maximum or minimum shear forces may vary.

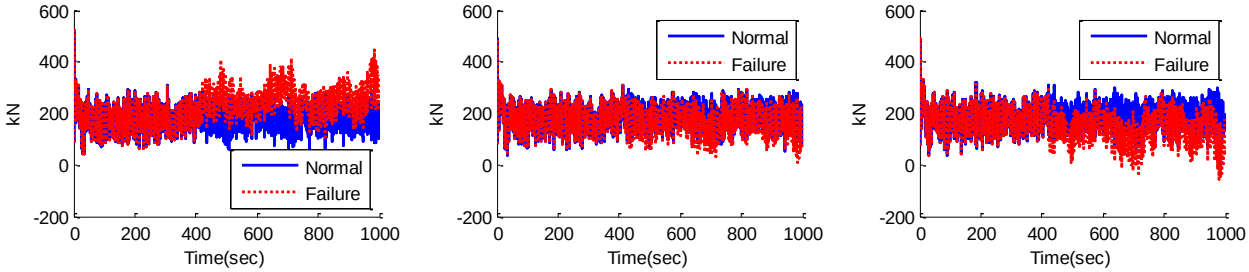

(a) Blade #1 (b) Blade #2 (c) Blade #3

Figure 12 Blade flapwise shear force with failure after 400 seconds

Table 7 Statistics of blade flapwise shear force with failure after 400 seconds

		Max.	Min	Mean	SD
Blade #1 (kN)	N	3.082E+02	5.948E+01	1.828E+02	4.250E+01
	B	4.474E+02	6.200E+01	2.283E+02	6.038E+01
Blade #2 (kN)	N	3.083E+02	5.253E+01	1.826E+02	4.243E+01
	B	3.093E+02	6.952E+00	1.680E+02	4.731E+01
Blade #3 (kN)	N	3.185E+02	4.328E+01	1.824E+02	4.315E+01
	B	3.185E+02	-5.337E+01	1.526E+02	5.442E+01

Other than the final blade pitch angle of failed blade and associated blade structural responses, the tower base loadings and the platform yaw response also show similar trend as already presented in Figures 7~10. Since aerodynamic loadings are unbalanced, same 1P response is detected in various responses of FOWT such as tower base torsional moment and platform yaw motion. The unbalanced loadings on the blades significantly reduce the fatigue life of the structural members, so it is important to check the structural integrity with various turbine failure scenarios.

4. CONCLUSIONS

The dynamic responses of a Hywind spar-type wind turbine with partially failed blade pitch control are investigated. Through this study, it is seen that the effect due to the partial failure of blade pitch control can be significant regardless of the final pitch angle. Specifically, the platform yaw response and the tower-base torsional moment are the most serious changes compared to the other responses. The associated turbine responses, such as tower-base loads and blade-root shear forces, are also checked with partially failed blade pitch control case. Due to the rotational imbalance with the failure, the 1P excitations and responses are more pronounced in the tower and blade dynamics. One of the interesting responses in this study is that the blade root shear forces of the two remaining blades show different mean and maximum loadings. This is because the platform-yaw-induced inertial loading on the blade could have some repetitive pattern during the simulation time. The repetitive behavior of inertial loading is strongly related with the overlap between the 1P platform yaw motion and the rotational motion of the rotor itself. The maximum root shear force of each blade occurs at a difference azimuth angle of the rotor depending on the blade position.

To avoid the local fatigue failure or entire system collapse due to the unbalanced loadings from the blades, the structural integrity, especially for the yaw-related responses, should be carefully checked. The present approach for FOWT can directly be applied to the development of remote structural health monitoring system in detecting partial failure of blade pitch control or imbalance loadings of the rotor by measuring tower or platform responses.

REFERENCES

Bae, Y.H., Kim, M.H., Shin, Y.S. (2010), "Rotor-floater-mooring coupled dynamic analysis of mini TLP-type offshore floating wind turbines". *In: Proceedings of the ASME 29th International Conference on Ocean, Offshore and Arctic Engineering*, Shanghai, China.

Bae, Y.H., Kim, M.H., (2013a), "Rotor-floater-tether coupled dynamics including second-order sum–frequency wave loads for a mono-column-TLP-type FOWT (floating offshore wind turbine)". *J. Ocean Engineering*, Vol. 61, 109-122.

Bae, Y.H., Kim, M.H. (2013b), "Coupled Dynamic Analysis of FOWT (Floating Offshore Wind Turbine) with Partially Broken Blade". *In: Proceedings of the 23rd International Offshore and Polar Engineering Conference*, Anchorage, AK.

Henderson, A., Leutz, R., Fujii, T. (2002), "Potential for floating offshore wind energy in Japanese waters". *In: Proceedings of the 12th International Offshore and Polar Engineering Conference*, Kitakyushu, Japan.

Henderson, A.R., Zaaijer, M., Bulder, B., Pierik, J., Huijsmans, R., van Hees, M., Snijders, E., Wijnants, G.H., Wolf, M.J. (2004), "Floating windfarms for shallow offshore sites". *In: Proceedings of the 22nd International Offshore and Polar Engineering Conference*, Toulon, France.

Jagdale, S., Ma, Q. (2010), "Practical simulation on motions of a TLP-type support structure for offshore wind turbines". *In: Proceedings of the 20th International Offshore and Polar Engineering Conference*, Beijing, China.

Jonkman, J.M., (2003), *Modeling of the UAE Wind Turbine for Refinement of FAST_AD*. National Renewable Energy Laboratory, Golden, CO.

Jonkman, J.M., Buhl Jr, M.L., (2004), *FAST user's guide*. National Renewable Energy Laboratory, Golden, CO.

Jonkman, J.M., Sclavounos, P.D. (2006)," Development of fully coupled aeroelastic and hydrodynamic models for offshore wind turbines". Paper presented at the 44th AIAA Aerospace Sciences Meeting and Exhibit, Reno, NV.

Jonkman, J.M., (2007), *Dynamics modeling and loads analysis of an offshore floating wind turbine*. National Renewable Energy Laboratory, Golden, CO.

Jonkman, J.M. (2008), "Influence of control on the pitch damping of a floating wind turbine". *In: Proceedings of the ASME Wind Energy Symposium*, Reno NV.

Kim, M.H., Tahar, A., Kim, Y.B. (2001), "Variability of TLP motion analysis against various design methodologies/parameters". *In: Proceedings of the 11th International Offshore and Polar Engineering, Stavanger*, Stavanger, Norway.

Lee, C.H., Newman, J.N., (1991), *First-and second-order wave effects on a submerged spheroid*.

Musial, W.D., Butterfield, S., Boone, A. (2004), "Feasibility of floating platform systems for wind turbines". *In: Proceedings of the 42nd AIAA Aerospace Sciences Meeting and Exhibit*, Reno, NV.

Nielsen, F.G., Hanson, T.D., Skaare, B. (2006), "Integrated dynamic analysis of floating offshore wind turbines". *In: Proceedings of the ASME 25th International Conference on Offshore Mechanics and Arctic Engineering*, Hamburg, Germany.

Roddier, D., Cermelli, C., Weinstein, A. (2009), "Windfloat: A floating foundation for offshore wind turbines part i: design basis and qualification process". *In: Proceedings of the ASME 28th International Conference on Ocean, Offshore and Arctic Engineering*, Honolulu, HI.

Tahar, A., Kim, M.H., (2003), "Hull/mooring/riser coupled dynamic analysis and sensitivity study of a tanker-based FPSO". *J. Applied Ocean Research*, Vol. 25 (6), 367-382.

Tong, K., (1998), "Technical and economic aspects of a floating offshore wind farm". *J. Wind Engineering and Industrial Aerodynamics*, Vol. 74, 399-410.

Withee, J.E. (2004), Fully coupled dynamic analysis of a floating wind turbine system. Doctoral thesis, Massachusetts Institute of Technology.

Yang, C.K., Kim, M., (2010), "Transient effects of tendon disconnection of a TLP by hull–tendon–riser coupled dynamic analysis". *J. Ocean Engineering*, Vol. 37 (8), 667-677.